Acta Geochim
https://doi.org/10.1007/s11631-024-00732-z

ORIGINAL ARTICLE

First discovery of the Late Triassic syenite and coeval epigenetic Cu mineralization in the Jianglang Dome, eastern Tibetan Plateau, China

Yanpei Dai[1] · Yudi Zhu[2] · Di Xiu[3] · Huihua Zhang[1] · Shengxian Liang[1] · Tongzhu Li[1] · Qing Zhou[1]

Received: 2 May 2024 / Revised: 5 August 2024 / Accepted: 13 August 2024

Abstract The Jianglang Dome has integral tectonostratigraphic units and contains a suite of high-grade stratiform Cu deposits. However, the formation mechanism of this dome and genetic model of Cu mineralization remain a matter of debate. The resolution of these problems hinges on the presence of magmatic intrusions in the core. Here, we report bulk geochemical and zircon U-Pb data of a newly discovered syenite intrusion as well as chalcopyrite Re-Os dating results. We aim to explore genesis of the Jianglang Dome, genetic model of the stratiform Cu deposits, and rare metal mineralization potential of the syenite intrusion. The dated syenite sample yields an emplacement age of 207.1 ± 2.0 Ma, which matches post-collisional extension in the Songpan-Ganze Orogen. The syenite rocks have average high (Zr + Nb + Ce + Y) concentrations of 512 ppm, 10000×Ga/Al ratios of 3.97, and crystallization temperatures of 827 °C, together with low Mg# values of 1.73; they fit the A-type granitoid definition and a crustal origin. Chalcopyrite separates yield a Re-Os isochron age of 207.1 ± 5.3 Ma, which markedly postdates the formation age of their ore-hosting rocks (the Liwu Group, ca. 553 Ma). Our new age determination, together with previous chalcopyrite Re–Os isochron age of ca. 151.1 Ma and sulfide sulfur isotope ($\delta^{34}S_{V\text{-}CDT}$ = 8.7‰–5.6‰) and tourmaline boron isotope ($\delta^{11}B$ = − 15.47‰ to − 5.91‰) data, confirms multistage epigenetic Cu mineralization related to magmatic-hydrothermal fluids. Compared with regional ca. 209–207 Ma fertile granitoids, the studied syenite intrusion shows unevolved and barren affinities and negligible rare metal mineralization potential. Combined with residual gravity low anomalies in the core of the Jianglang Dome, which suggest a large deep-seated granitic batholith, we prefer thermal doming resulting from magma-induced uplift for the nature of this dome.

Keywords Syenite intrusion · Zircon U-Pb dating · Chalcopyrite Re-Os dating · Epigenetic mineralization · Stratiform Cu deposits · Jianglang Dome

1 Introduction

The Songpan-Ganze Orogen (SGO) occupies a large area of the eastern Tibetan Plateau (Fig. 1a), and numerous isolated domes have been identified in its eastern margin. Among them, the Jianglang Dome is the most representative with the most complete tectonostratigraphic units (Yan et al. 1997, 2003a); however, its formation mechanism has been controversial. For instance, Hou (1996) and Hou and Fu (2002) proposed it as a structural dome, which was formed by overlapping of duplex compression and contraction. In contrast, Yan et al. (1997) assigned it as a metamorphic core complex associated with magma-induced uplift caused by lithospheric thermal anomalies. To date, direct evidence of magma-induced doming is still lacking in the core of the Jianglang Dome. During recent field geological mapping, a syenite intrusion was first discovered in this area (Fig. 1b) and was probably responsible for doming.

Furthermore, a suite of high-grade (average 1.75%) stratiform Cu deposits occurs in the core of the

✉ Yudi Zhu
420132343@qq.com

1 Chengdu Center, China Geological Survey (Geosciences Innovation Center of Southwest China), Ministry of Natural Resources, Chengdu 610218, China

2 School of Geoscience and Technology, Southwest Petroleum University, Chengdu 610500, China

3 Regional Geological Survey Institute of Hebei Province (Geotourism Research Center of Hebei Province), Langfang 065000, China

Published online: 28 August 2024

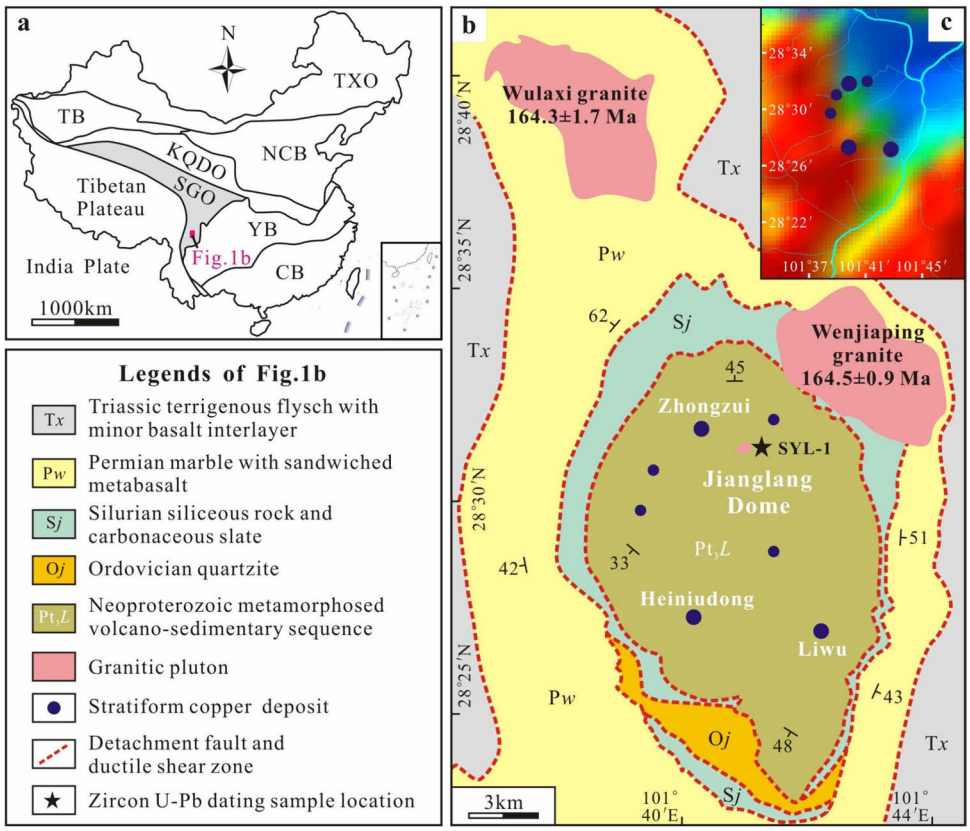

Fig. 1 **a** Simplified tectonic division map of China, TXO = Tianshan-Xingmeng Orogen, TB. Tarim Block, NCB. North China Block, KQDO. Kunlun-Qinling-Dabie Orogen, SGO. Songpan-Ganze Orogen, YB. Yangtze Block, CB. Cathaysia Block. **b** Geological map of the Jianglang Dome. **c** The residual gravity anomaly map of the Jianglang Dome and its vicinity; note that warm colors indicate high gravity, while cool colors indicate low gravity

Jianglang Dome, hosted by the Neoproterozoic Liwu Group (Fig. 1b), which is a metamorphosed volcano-sedimentary sequence. These deposits are one of the most important copper resource producers in southwest China (Dai et al. 2016). Due to overall paucity of ore-related minerals amenable to reliable isotopic dating, diverse syngenetic and epigenetic models have been suggested over the years, including: (1) a sedimentary exhalative origin overprinted by metamorphism (Yao 1990); (2) volcanogenic massive sulfide deposits superposed by deformation and metamorphism (Li et al. 2012); (3) a tectono-stratabound hydrothermal origin (Yan et al. 2003b); (4) a metamorphic hydrothermal origin (Ma et al. 2010); and (5) a (post-) magmatic hydrothermal origin (Chen et al. 2011; Zhou et al. 2017). These contrasting genetic models have hindered current mineral exploration, and establishing a correct mineralization model is crucial.

In this study, we employed integrated whole-rock geochemical and zircon U-Pb isotopic analyses of the newly discovered syenite intrusion as well as chalcopyrite Re–Os dating of the stratiform Cu deposits to determine genesis of the Jianglang Dome, genetic model of the stratiform Cu deposits, and rare metal mineralization potential of the syenite intrusion.

2 Regional geology

The SGO resulted from interactions between the Yangtze, North China, and Qiangtang Blocks (Fig. 1a) during the Middle to Late Triassic closure of the Paleo-Tethys Ocean, which induced accretionary orogeny (Roger et al. 2010; Yan et al. 2018a, b). It is exclusively filled by a 5–15-km-thick Triassic flysch that received materials from adjacent blocks (Weislogel et al. 2010). These flysch deposits underwent greenschist to amphibolite facies Barrovian metamorphism at 205–190 Ma (Huang et al. 2003a, b) and were intruded by widespread granitic plutons (Roger et al. 2010). Combined with tectonic evolution of the SGO, these granitoids were classified into syn- to late-orogenic/post-collisional (ca. 220–200 Ma) and post-orogenic (ca. 200–150 Ma) varieties (Roger et al. 2010). Among them, late- and post-orogenic granitoids were likely associated with thickened lower crust, lithospheric delamination, and asthenospheric upwelling, accompanied by 220–150 Ma extentional tectonics (Zhang et al. 2007; Roger et al. 2010).

More than ten isolated domes were distributed along the eastern SGO, with medium- to high-grade metamorphic complexes in their cores (Yan et al. 1997). The Jianglang Dome consists of three tectonostratigraphic units, including:

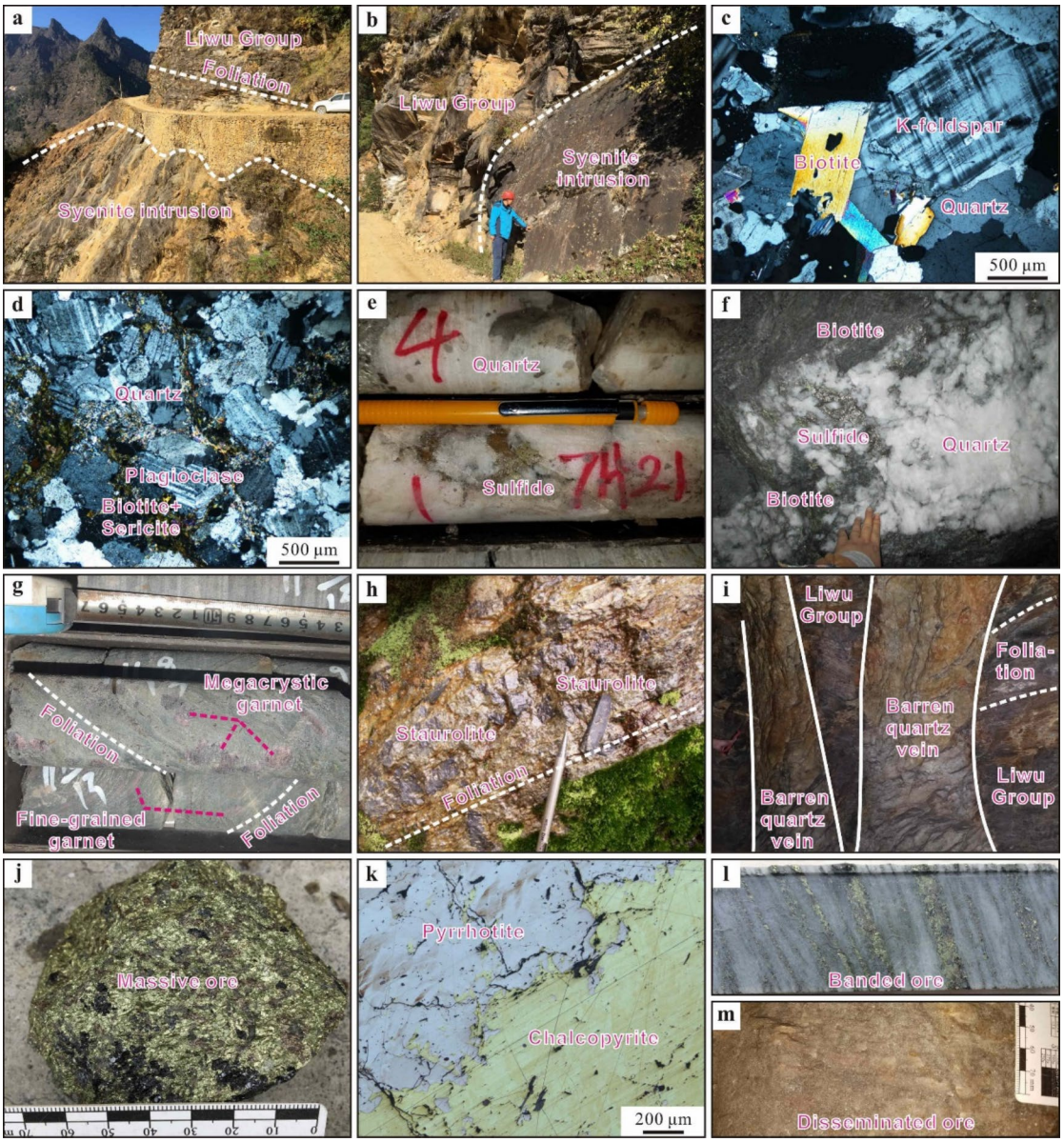

Fig. 2 **a**, **b** Field occurrence of syenite that intrudes the Liwu Group; **c**, **d** micrographs of syenite dating sample SYL-1; **e**, **f** first stage of coexisting silicic and biotitic alteration; **g** first stage of fine-grained garnet and second stage of megacrystic garnet; **h** second stage of megacrystic staurolite; **i** late stage of non-mineralized quartz veins crosscutting foliation; **j**, **k** hand specimens and micrographs of massive ores; **l**, **m** banded and disseminated ores

(1) a core complex known as the Liwu Group, (2) an overlying middle slab of the Paleozoic metamorphosed volcano-sedimentary sequences, and (3) a sedimentary cover of the Triassic Xikang Group (Yan et al. 1997, 2003a). These units are separated by ring detachment faults or ductile shear zones (Fig. 1b). The Liwu Group is a metamorphosed volcano-sedimentary sequence with a total thickness of > 3600 m and mainly comprises two-mica quartz schist, quartzite, and minor sandwiched metabasic rocks. Previous studies obtained a weighted mean $^{206}Pb/^{238}U$ age of 552.8 ± 5.7 Ma for the youngest magmatic zircons within quartzite, and interpreted it as the formation age of the Liwu Group (Li et al. 2016). The middle slab is composed of (1) the Ordovician Jianglang Formation of quartzite, (2) the Silurian Jiaba Formation of siliceous rock, carbonaceous slate, and minor metabasalt interlayer, and (3) the Late Permian Wulaxi Formation of marble with sandwiched metabasalt (Zhu et al. 2020).

Besides, the Wenjiaping and Wulaxi granitic plutons are developed in the north of the Jianglang Dome (Fig. 1b) and intrude the Liwu Group, Jiaba Formation, and Wulaxi Formation. Previous LA-ICP-MS zircon U-Pb dating

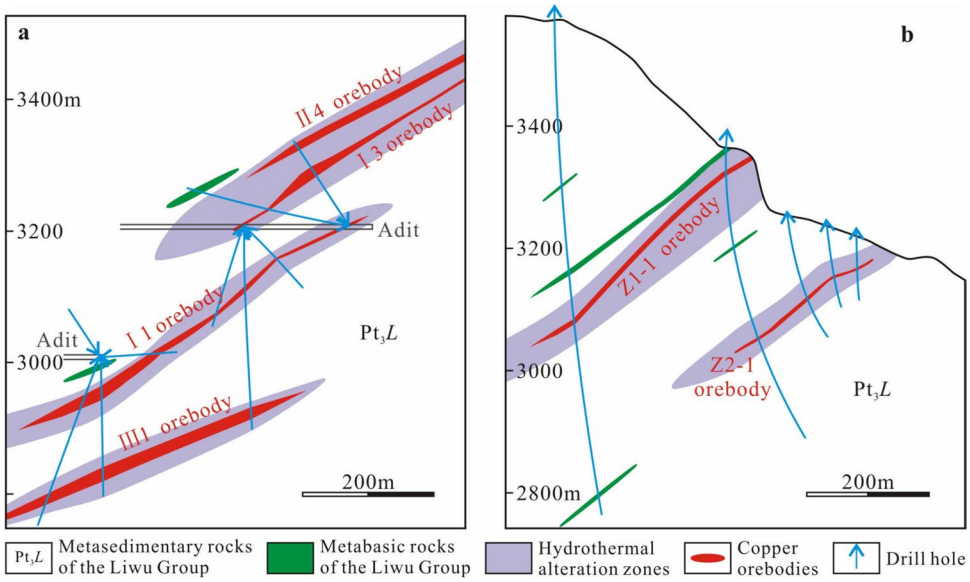

Fig. 3 Typical exploration lines of the Heiniudong **a** and Zhongzui **b** stratiform Cu deposits

indicates their emplacement ages of 164.5 ± 0.9 Ma and 164.3 ± 1.7 Ma. Geochemical and zircon Hf isotope data are suggestive of a post-orogenic extensional setting and a main derivation from ancient continental crust (Dai et al. 2017). According to the gravity data we have recently obtained, the core of the Jianglang Dome shows residual gravity low anomalies (Fig. 1c), indicating that there might be a large concealed granitic batholith in the deep (e.g., Mangkhemthong et al. 2020). During recent field geological mapping, a syenite intrusion was newly discovered in the northern core of the Jianglang Dome, near the Zhongzui deposits (Fig. 1b). It clearly intrudes the Liwu Group and shows typically massive structure (Fig. 2a, b).

3 Deposit geology

Several stratiform Cu deposits occur within the Liwu Group that occupies the core of the Jianglang Dome, typified by Liwu, Heiniudong, and Zhongzui (Fig. 1b). They are one of the most important copper resource producers in southwest China and have an average Cu grade of ~ 1.75% with erratic high grade up to ~ 20%. These deposits show uniformities in alteration type, mineralization style, and mineral assemblage and were collectively referred to as "Liwu-type" high-grade Cu deposits (Dai et al. 2016).

The alteration envelopes in these stratiform Cu deposits are bedding-parallel (Fig. 3) and are dominated by silicic, biotitic, sericitic, and chloritic alteration, with minor (total < 10 vol%) garnet, tourmaline, and staurolite. The hydrothermal alteration can be divided into three stages according to the paragenetic sequence of minerals: (1) first stage responsible for Cu mineralization, comprising coexisting silicic, biotitic, sericitic, and chloritic alteration as well as fine-grained tourmaline and garnet (Fig. 2e–g); (2) second stage characterized by megacrystic garnet, tourmaline, and staurolite (Fig. 2g, h), which were likely related to post-magmatic high-temperature solutions; (3) late stage represented by non-mineralized quartz and calcite veins crosscutting foliation (Fig. 2i).

Three distinct styles of sulfide mineralization are identified in these stratiform Cu deposits: (1) massive with a high grade of > 5% Cu (Fig. 2j, k); (2) banded with a medium grade of 5–1% Cu (Fig. 2l); (3) disseminated with a low grade of < 1% Cu (Fig. 2m). The metal sulfides are dominated by chalcopyrite and pyrrhotite, with minor sphalerite and pyrite. The Cu orebodies in the Liwu, Heiniudong, and Zhongzui deposits all occur in hydrothermal alteration envelopes. Specifically, in the Heiniudong deposit, four orebodies were identified based on mineral exploration from top to bottom (Fig. 3a): II4 orebody with an extension of ~ 250 m, I3 main orebody extending > 900 m, I1 orebody with an extension of ~ 700 m, and III1 orebody extending > 350 m. In the Zhongzui deposit, two hydrothermal alteration envelopes were discovered based on geologic mapping and drill cores. They contain two layers of orebodies, including the upper Z1-1 orebody with an extension of > 3.50 km and the lower Z2-1 orebody extending ~ 1.0 km (Fig. 3b).

4 Analytical methods

We collected five syenite intrusion samples as well as five massive ore samples from the Zhongzui and Heiniudong Cu deposits. Their sample locations are marked in Fig. 1b and listed in Table 4. The rock samples are mainly composed of ~ 35 vol% plagioclase, ~ 30 vol% K-feldspar, ~ 25 vol% quartz, ~ 10 vol% biotite, and < 2 vol% sericite (Fig. 2c–d).

Table 1 Whole-rock major (wt%) and trace element (ppm) data of syenite samples in the Jianglang Dome

Sample	SYL-1	SYL-2	SYL-3	SYL-4	SYL-5
SiO_2	59.46	61.21	61.40	59.85	59.67
TiO_2	0.64	0.50	0.56	0.63	0.65
Al_2O_3	14.30	14.73	14.70	14.64	14.70
$Fe_2O_3^T$	10.96	9.27	9.64	10.64	10.60
MnO	0.30	0.26	0.25	0.30	0.29
MgO	0.13	0.07	0.06	0.10	0.10
CaO	3.10	2.88	2.59	2.97	3.08
Na_2O	4.67	5.24	4.92	4.76	4.71
K_2O	5.12	5.04	5.35	5.31	5.48
P_2O_5	0.14	0.10	0.10	0.14	0.14
LOI	0.19	0.60	0.56	0.16	0.27
Total	99.01	99.90	100.13	99.50	99.69
A/NK	1.08	1.05	1.06	1.08	1.07
A/CNK	0.76	0.76	0.79	0.77	0.76
$Mg^{\#}$	2.30	1.48	1.22	1.83	1.84
La	37.7	50.9	53.3	45.1	42.9
Ce	80.0	104.0	108.5	92.9	86.5
Pr	10.2	12.0	13.0	10.9	10.3
Nd	42.2	49.9	53.7	44.8	44.0
Sm	9.69	10.90	11.25	9.55	9.56
Eu	3.43	3.53	3.64	3.81	3.83
Gd	9.15	11.15	11.10	9.62	9.20
Tb	1.44	1.73	1.68	1.41	1.40
Dy	9.05	9.98	9.83	8.38	7.95
Ho	1.69	2.01	1.98	1.64	1.65
Er	5.18	5.47	5.81	4.83	4.57
Tm	0.67	0.83	0.81	0.65	0.68
Yb	4.60	4.91	5.16	4.34	4.21
Lu	0.75	0.85	0.84	0.75	0.74
ΣREE	216	268	281	239	227
$(La/Yb)_N$	5.5	7.0	7.0	7.0	6.9
Eu/Eu*	1.10	0.97	0.98	1.20	1.23
Rb	78.9	71.0	76.2	83.3	83.7
Sr	24.5	33.4	32.9	25.6	25.1
Ba	637	454	482	657	649
Nb	48.5	57.1	63.1	48.0	48.2
Ta	2.60	3.20	3.00	2.30	2.40
Zr	284	386	395	267	258
Hf	7.10	9.50	9.30	7.10	6.30
Th	4.11	6.06	6.07	4.09	4.13
U	1.17	1.39	1.43	0.97	1.06
Cs	3.36	1.28	1.34	3.73	3.24
Ga	28.4	32.6	33.8	30.2	28.7
Y	43.9	51.6	52.6	44.2	43.3
10,000 × Ga/Al	3.75	4.18	4.34	3.90	3.69
Zr + Nb + Ce + Y	456	599	619	452	436
T_{Zr} (°C)	693	727	740	691	684

(1) $Fe_2O_3^T$ is total Fe, and LOI is loss on ignition. (2) A/NK = molar $Al_2O_3/(Na_2O + K_2O)$; A/CNK = molar $Al_2O_3/(CaO + Na_2O + K_2O)$. (3) Mg# = 100×Mg/(Mg + ΣFe^{2+}) in mole. (4) $Eu/Eu^* = 2Eu_N/(Sm_N + Gd_N)$, and normalized values of chondrite after Taylor and Mclennan (1985). (5) T_{Zr} (°C) is zircon saturation temperature calculated using the geothermometer of Boehnke et al. (2013)

The massive ore samples chiefly comprise ~ 30 vol% chalcopyrite, ~ 40 vol% pyrrhotite, ~ 20 vol% quartz, and ~ 10 vol% sphalerite (Fig. 2j, k).

Rock samples were crushed for zircon separation (80 mesh) as well as whole-rock geochemical analysis (200 mesh). Ore samples were crushed into 80 mesh for chalcopyrite separation. Zircon and chalcopyrite were separated using conventional heavy liquid and magnetic techniques and then were hand-picked under a binocular microscope at the Regional Geological Survey Institute of Hebei Province (Geotourism Research Center of Hebei Province), Langfang, China.

Whole-rock major and trace elements were analyzed using the ME-XRF26 and ME-MS81 methods at the Analytical Laboratory of ALS Chemex (Guangzhou) Company Limited. Major oxides were measured using a PANalytical Axios-advance (Axios PW4400) x-ray fluorescence spectrometer, with analytical precision < 5%. Trace element measurements were performed using a Perkin-Elmer Elan 9000 ICP-MS, with precision > 10%.

Zircon cathodoluminescent images were taken to examine internal textures and morphology. U-Pb isotopes and trace elements were synchronously analyzed using an Agilent 7900 ICP-MS instrument equipped with an excimer laser ablation system at the Wuhan SampleSolution Analytical Technology Co., Ltd. Zircon standards GJ-1 (601.95 ± 0.4 Ma, Horstwood et al. 2016) and Plešovice (337.13 ± 0.13 Ma, Sláma et al. 2008) were used to monitor the precision and accuracy. They yielded mean $^{206}Pb/^{238}U$ ages of 601.8 ± 2.8 Ma ($n = 4$) and 338.1 ± 1.9 Ma ($n = 4$). Detailed operating conditions and procedures followed those in Liu et al. (2008).

Chalcopyrite Re-Os dating was performed at the National Research Center of Geoanalysis, Chinese Academy of Geological Sciences. Re and Os concentrations and isotope ratios were determined using negative thermal ionization mass spectrometry. A chalcopyrite standard GBW04477/JCBY was used to control reproducibility and instrument stability (Du et al. 2012), and detailed analytical procedures followed those in Du et al. (2004). Re-Os isochron ages were calculated using the online IsoplotR program (Vermeesch 2018).

5 Results

5.1 Major and trace elements

Whole-rock geochemical data of the investigated felsic intrusion are listed in Table 1. In detail, the samples yield SiO_2 of 59.46 wt%–61.40 wt%, Al_2O_3 of 14.30 wt%–14.73 wt%, $Fe_2O_3^T$ of 9.27 wt%–10.96 wt%, Na_2O of 4.67 wt%–5.24 wt%, and K_2O of 5.04 wt%–5.48 wt%. They

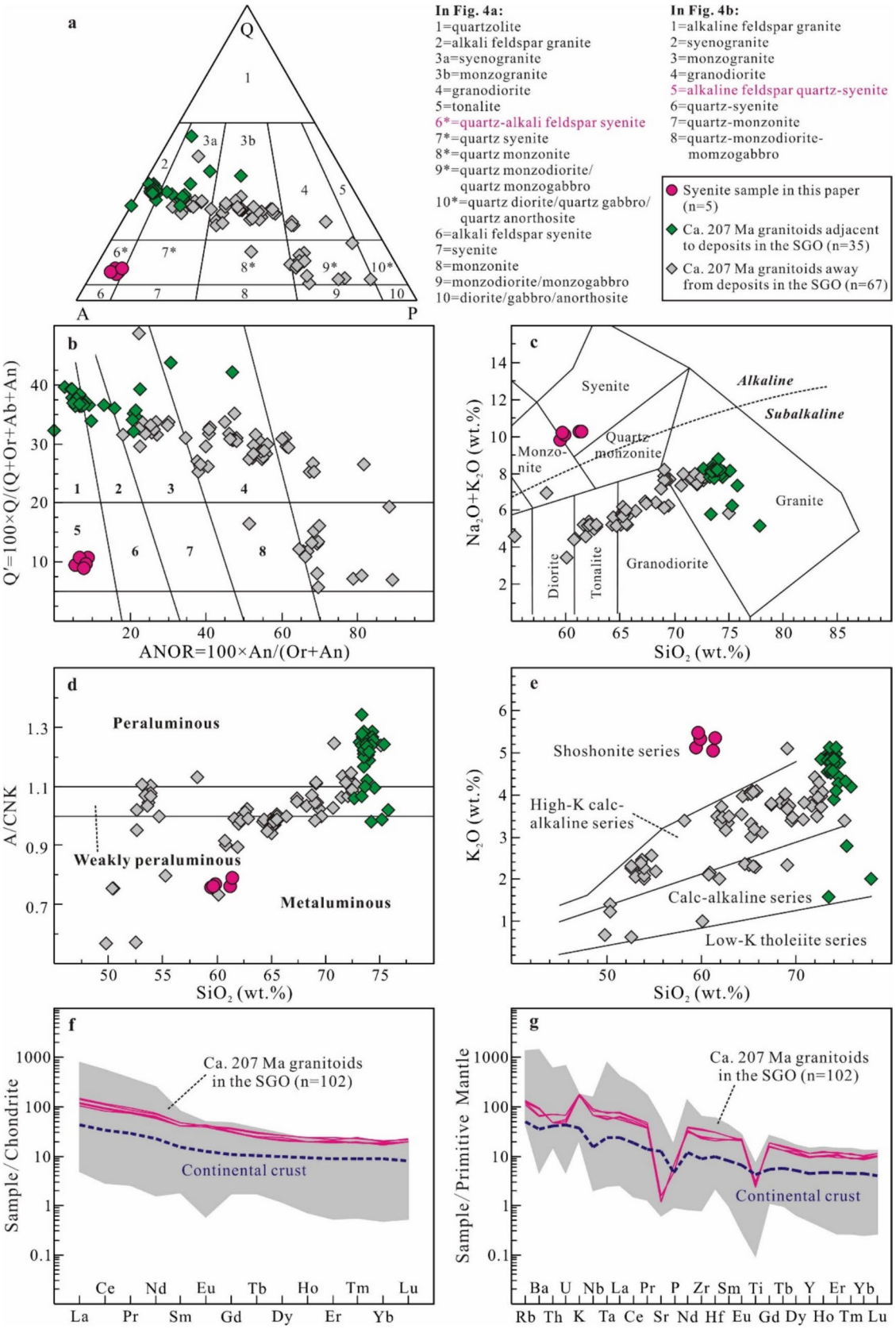
a
Q
A
P
1
2
3a
3b
4
5
6*
7*
8*
9*
10*
6
7
8
9
10
In Fig. 4a:
1=quartzolite
2=alkali feldspar granite
3a=syenogranite
3b=monzogranite
4=granodiorite
5=tonalite
6*=quartz-alkali feldspar syenite
7*=quartz syenite
8*=quartz monzonite
9*=quartz monzodiorite/ quartz monzogabbro
10*=quartz diorite/quartz gabbro/ quartz anorthosite
6=alkali feldspar syenite
7=syenite
8=monzonite
9=monzodiorite/monzogabbro
10=diorite/gabbro/anorthosite
In Fig. 4b:
1=alkaline feldspar granite
2=syenogranite
3=monzogranite
4=granodiorite
5=alkaline feldspar quartz-syenite
6=quartz-syenite
7=quartz-monzonite
8=quartz-monzodiorite-momzogabbro
Syenite sample in this paper (n=5)
Ca. 207 Ma granitoids adjacent to deposits in the SGO (n=35)
Ca. 207 Ma granitoids away from deposits in the SGO (n=67)
b
Q'=100×Q/(Q+Or+Ab+An)
ANOR=100×An/(Or+An)
c
Syenite
Alkaline
Subalkaline
Monzo-nite
Quartz monzonite
Granite
Granodiorite
Diorite
Tonalite
Na2O+K2O (wt.%)
SiO2 (wt.%)
d
Peraluminous
Weakly peraluminous
Metaluminous
A/CNK
SiO2 (wt.%)
e
Shoshonite series
High-K calc-alkaline series
Calc-alkaline series
Low-K tholeiite series
K2O (wt.%)
SiO2 (wt.%)
f
Ca. 207 Ma granitoids in the SGO (n=102)
Continental crust
Sample/Chondrite
Ce Nd Eu Tb Ho Tm Lu
La Pr Sm Gd Dy Er Yb
g
Ca. 207 Ma granitoids in the SGO (n=102)
Continental crust
Sample/Primitive Mantle
Ba U Nb La Pr P Zr Sm Ti Tb Y Er Yb
Rb Th K Ta Ce Sr Nd Hf Eu Gd Dy Ho Tm Lu

◂**Fig. 4** **a** Quartz-alkali feldspar-plagioclase (QAP) diagram (after Le Maitre 2002); **b** Q′ vs. ANOR diagram (after Streckeisen and Le Maitre 1979); **c** total alkali vs. silica (TAS) diagram (after Middlemost 1994), with the dashed line from Irvine and Baragar (1971); **d** molar $Al_2O_3/(CaO+Na_2O+K_2O)$ vs. SiO_2 diagram; **e** K_2O vs. SiO_2 diagram (after Peccerillo and Taylor 1976); **f** chondrite-normalized REE patterns; **g** primitive mantle-normalized trace element profiles. Values of chondrite, continental crust, and primitive mantle after Taylor and Mclennan (1985) and Sun and McDonough (1989). Data of ca. 207 Ma granitoids adjacent to deposits including ca. 207 Ma Majingzi two-mica granite ($n=21$, Zhang et al. 2022; Zhao et al. 2022) and ca. 209 Ma Ke'eryin aplite ($n=14$, Li et al. 2022; Fei et al. 2023). Data of ca. 207 Ma granitoids away from deposits including ca. 205 Ma Taiyanghe monzonite ($n=17$, Yuan et al. 2010; Deschamps et al. 2017), ca. 209 Ma Tagong monzogranite ($n=15$, Chen et al. 2017), ca. 210–205 Ma Jinsha suture granodiorite ($n=16$, Liu et al. 2019), and ca. 207 Ma Riluku monzogranite ($n=19$, Zhan et al. 2020)

have A/CNK ratios [molar $Al_2O_3/(CaO+Na_2O+K_2O)$] of 0.76–0.79 and Mg# values [molar $100\times Mg/(Mg+\Sigma Fe^{2+})$] of 1.22–2.30. Specially, QAP, Q′ versus ANOR and (Na_2O+K_2O) versus SiO_2 versus diagrams indicate that they are syenite in composition (Fig. 4a–c). Furthermore, A/CNK versus SiO_2 and K_2O versus SiO_2 diagrams suggest their metaluminous and shoshonite series affinities (Fig. 4d, e).

The rock samples have ΣREE contents of 216–281 ppm and Eu/Eu* values of 0.97–1.23 calculated using chondritic data. Several rare earth elements and trace elements are present in higher abundances than other elements, such as La (37.7–53.3 ppm), Ce (80.0–109 ppm), Nd (42.2–53.7 ppm), Rb (71.0–83.7 ppm), Ba (454–657 ppm), and Zr (258–395 ppm). Furthermore, all the rocks are LREE-enriched on chondrite-normalized diagram, with $(La/Yb)_N$ values of 5.5–7.0 calculated using chondritic data. Their primitive mantle-normalized trace element spidergram shows significant enrichment in large ion lithophile elements (e.g., Rb and K) and depletion in Sr and high-field-strength elements (e.g., Ti). All these geochemical signatures are broadly comparable to the continental crust and ca. 207 Ma granitoids in the SGO (Fig. 4f, g).

5.2 Zircon U-Pb dating

A total of 17 zircon grains were analyzed, and the dating results are provided in Tables 2 and 3. The zircons are angular and prismatic and show dull cathodoluminescent images without apparent oscillatory zoning (Fig. 5a). Their Th/U ratios range between 0.20 and 3.33 (mostly > 0.5), with an average of 1.10 (Fig. 5b). They have ΣREE contents of 1151–2428 ppm, Ce/Ce*values of 1.16–3.92, and Eu/Eu* values of 0.32–0.88, showing obvious HREE-enriched patterns (Fig. 5c).

The zircons are plotted on or near the concordia curve (Fig. 6a), with $^{206}Pb/^{238}U$ ages of 214.0–198.7 Ma. They have a weighted mean age of 207.1 ± 2.0 Ma (MSWD = 4.3), and this is the best estimate for their crystallization age.

5.3 Chalcopyrite Re-Os dating

Chalcopyrite Re-Os isotope data are shown in Table 4. Five chalcopyrite separates from the Zhongzui and Heiniudong deposits exhibit variable Re (2.364–6.684 ppb) and Os (0.0044–0.0302 ppb) concentrations. They have $^{187}Re/^{188}Os$ ratios of 423.8–2827.9 and $^{187}Os/^{188}Os$ ratios of 7.123–15.424. Their data points yield an isochron age of 207.1 ± 5.3 Ma and an initial $^{187}Os/^{188}Os$ of 5.766 ± 0.075 (MSWD = 2.5, Fig. 6b).

6 Discussion

6.1 Petrogenesis of the newly discovered syenite intrusion

Zircon commonly contains various trace elements that are sensitive to its formation condition. Grimes et al. (2007) introduced U/Yb versus Hf and U/Yb versus Y diagrams to distinguishing zircon provenance of continental or ocean crust environments. These discrimination diagrams provide a continental derivation for our dated zircons (Fig. 7a, b). They have high Th/U ratios, positive Ce anomalies, negative Eu anomalies, and HREE-enriched patterns (Fig. 5b, c), indicating a dominantly magmatic origin (Hoskin and Schaltegger 2003). Noticeably, their dull cathodoluminescent images are atypical, without oscillatory zoning, which is likely attributed to hydrothermal alteration. Hoskin (2005) adopted $(Sm/La)_N$ versus La diagram to discriminate hydrothermal and magmatic zircons. However, many natural zircons were plotted between these two categories (Fig. 7c), and geochemical criteria for distinguishing hydrothermal and magmatic varieties were questioned as insufficient (Bell et al. 2019). More recently, Bell et al. (2016) investigated Jack Hills zircons of Western Australia and defined quantitative criteria of Light Rare Earth Element Index (LREE-I = Dy/Nd + Dy/Sm) for recognizing hydrothermal alteration. They proposed that hydrothermally altered zircons have low LREE-I values of < 30, while unaltered magmatic zircon compositions show high LREE-I values of > 30 (Bell et al. 2016, 2019). In this contribution, the dated zircons have LREE-I values of 367–28 with an average of 123 (Fig. 7d), implying insignificant hydrothermal impacts on these zircons. This is supported by low LOI (loss on ignition) values of 0.60–0.16 according to bulk geochemical data (Table 1). Taken together, our dated zircons within the studied syenite

Table 2 Trace and rare earth element data (ppm) of analyzed zircons within syenite sample SYL-1 in the Jianglang Dome

Spot	Th	U	Th/U	Ti	T (°C)	P	Nb	Ta	Y	Hf	La	Ce	Pr	Nd	Sm	Eu	Gd	Tb	Dy	Ho	Er	Tm	Yb	Lu	ΣREE	Ce/Ce*	Eu/Eu*	LREE-I
01	1317	1139	1.16	7.48	716	409	210	139	2634	6358	1.53	9.70	1.33	10.4	8.19	2.21	33.3	12.5	181	82.6	392	74.7	546	84.3	1439	1.46	0.35	39
03	973	1450	0.67	29.0	844	277	103	72.2	8076	6797	1.92	14.0	1.61	12.3	9.75	2.68	46.2	16.1	216	90.9	395	68.2	473	69.4	1417	1.72	0.32	40
04	2713	2169	1.25	17.2	791	240	116	52.5	2337	5915	0.29	2.55	0.40	1.61	1.47	0.89	8.82	5.15	113	69.4	407	95.1	861	158	1725	1.43	0.58	147
05	422	1520	0.28	8.92	731	259	250	212	2951	7955	1.68	17.8	2.26	15.5	7.12	1.46	18.1	7.83	138	78.1	454	101	856	130	1828	1.76	0.37	28
07	996	1356	0.74	26.1	833	145	104	18.1	2851	7831	0.17	1.21	0.095	0.89	0.57	0.51	6.63	5.40	128	82.7	495	118	1134	224	2197	2.19	0.49	367
08	963	2179	0.44	29.5	846	254	127	49.8	3567	7185	0.23	2.73	0.20	1.42	1.26	0.87	10.7	6.88	153	97.0	569	131	1224	230	2428	2.73	0.50	229
10	7339	3731	1.97	34.2	862	355	79.4	27.4	3472	5876	0.35	2.16	0.19	1.24	1.20	1.23	12.2	7.22	163	101	561	119	1017	175	2163	1.94	0.63	268
13	913	1587	0.58	17.4	792	564	93.0	82.7	2480	6913	2.54	12.5	2.15	12.8	6.15	2.40	12.9	5.91	117	71.5	419	87.9	679	107	1538	1.16	0.80	28
14	3207	1349	2.38	106	1001	233	2433	292	4735	7553	0.63	4.31	0.52	3.75	1.79	1.24	7.52	4.07	87.0	54.1	308	67.6	573	98.4	1212	1.62	0.88	72
15	2742	1479	1.85	86.5	974	839	159	214	2399	6264	1.70	8.41	1.27	8.44	4.63	1.79	14.8	6.64	122	70.5	396	87.6	734	125	1583	1.26	0.60	41
21	8253	2479	3.33	27.6	839	959	165	165	2520	7258	1.54	11.3	1.32	9.49	5.96	1.85	19.8	7.97	127	67.4	384	84.9	697	105	1525	1.70	0.47	35
23	2632	2931	0.90	18.5	798	164	112	102	2294	7044	0.15	1.72	0.070	0.77	1.02	0.48	5.62	3.93	101	68.4	406	88.1	725	121	1523	3.92	0.49	229
24	752	2068	0.36	6.82	708	298	111	70.4	1433	6323	0.46	2.96	0.38	2.97	1.71	0.77	6.56	3.31	66.7	44.1	293	74.6	749	146	1393	1.54	0.62	62
26	334	1679	0.20	23.3	821	172	96.0	44.8	1694	6166	1.91	5.43	0.42	1.68	0.66	0.63	4.21	2.99	71.4	47.7	284	64.7	566	99.0	1151	1.38	0.87	150
27	1268	1655	0.77	31.7	854	194	121	64.2	2415	7853	1.80	6.08	0.73	3.45	1.56	0.87	9.06	5.74	122	74.4	419	95.5	882	170	1792	1.25	0.55	114
28	3276	1929	1.70	17.2	791	419	216	91.1	3414	7271	0.40	4.35	0.22	1.74	1.65	1.09	13.2	7.52	155	91.0	501	104	839	133	1853	3.41	0.50	184
30	332	1515	0.22	33.6	860	315	77.9	44.2	1574	7089	0.93	5.67	0.68	4.72	2.14	1.07	8.24	3.79	74.2	45.7	275	65.8	600	109	1197	1.57	0.68	50

(1) T (°C) is Ti-in-zircon temperature calculated as in Watson et al. (2006). (2) $Ce/Ce^* = 2Ce_N/(La_N + Pr_N)$, $Eu/Eu^* = 2Eu_N/(Sm_N + Gd_N)$, normalized values of chondrite after Taylor and Mclennan (1985). (3) LREE-I = Dy/Nd + Dy/Sm (Bell et al. 2016, 2019)

Table 3 Zircon U-Pb dating results of syenite sample SYL-1 in the Jianglang Dome

Spot	Isotope ratios						Rho	Age (Ma)						Concordance (%)
	$^{207}Pb/^{206}Pb$	±σ	$^{207}Pb/^{235}U$	±σ	$^{206}Pb/^{238}U$	±σ		$^{207}Pb/^{206}Pb$	±σ	$^{207}Pb/^{235}U$	±σ	$^{206}Pb/^{238}U$	±σ	
SYL-1–01	0.0521	0.0012	0.2371	0.0054	0.0329	0.0003	0.4002	287.1	51.8	216.1	4.4	208.8	1.9	96
SYL-1–03	0.0514	0.0011	0.2371	0.0054	0.0333	0.0003	0.3429	261.2	50.0	216.0	4.4	211.1	1.6	97
SYL-1–04	0.0509	0.0009	0.2311	0.0043	0.0328	0.0003	0.4920	235.3	40.7	211.1	3.6	208.3	1.9	98
SYL-1–05	0.0514	0.0010	0.2351	0.0045	0.0331	0.0003	0.4362	257.5	42.6	214.4	3.7	209.9	1.7	97
SYL-1–07	0.0514	0.0011	0.2398	0.0051	0.0337	0.0003	0.4519	257.5	48.1	218.2	4.2	214.0	2.0	98
SYL-1–08	0.0469	0.0009	0.2111	0.0040	0.0326	0.0002	0.3789	42.7	44.4	194.5	3.3	206.7	1.5	93
SYL-1–10	0.0487	0.0008	0.2210	0.0038	0.0328	0.0003	0.5375	200.1	40.7	202.7	3.2	207.9	1.9	97
SYL-1–13	0.0493	0.0010	0.2240	0.0044	0.0329	0.0003	0.4516	161.2	41.7	205.2	3.6	208.5	1.8	98
SYL-1–14	0.0480	0.0012	0.2129	0.0052	0.0322	0.0004	0.4990	101.9	61.1	195.9	4.3	204.3	2.4	95
SYL-1–15	0.0507	0.0011	0.2355	0.0054	0.0335	0.0003	0.4244	233.4	50.0	214.7	4.5	212.6	2.1	98
SYL-1–21	0.0482	0.0010	0.2126	0.0043	0.0319	0.0003	0.5385	105.6	48.1	195.7	3.6	202.7	2.2	96
SYL-1–23	0.0516	0.0010	0.2290	0.0046	0.0320	0.0003	0.4537	333.4	50.9	209.4	3.8	203.3	1.8	97
SYL-1–24	0.0522	0.0010	0.2256	0.0055	0.0313	0.0005	0.7033	300.1	44.4	206.6	4.5	198.7	3.3	96
SYL-1–26	0.0471	0.0009	0.2111	0.0041	0.0324	0.0003	0.4490	57.5	46.3	194.5	3.4	205.4	1.8	94
SYL-1–27	0.0527	0.0011	0.2308	0.0051	0.0317	0.0003	0.4941	316.7	50.0	210.8	4.2	201.3	2.2	95
SYL-1–28	0.0499	0.0009	0.2189	0.0038	0.0317	0.0002	0.4521	190.8	40.7	201.0	3.2	201.3	1.6	99
SYL-1–30	0.0496	0.0010	0.2264	0.0045	0.0330	0.0003	0.4457	176.0	46.3	207.2	3.8	209.5	1.8	98

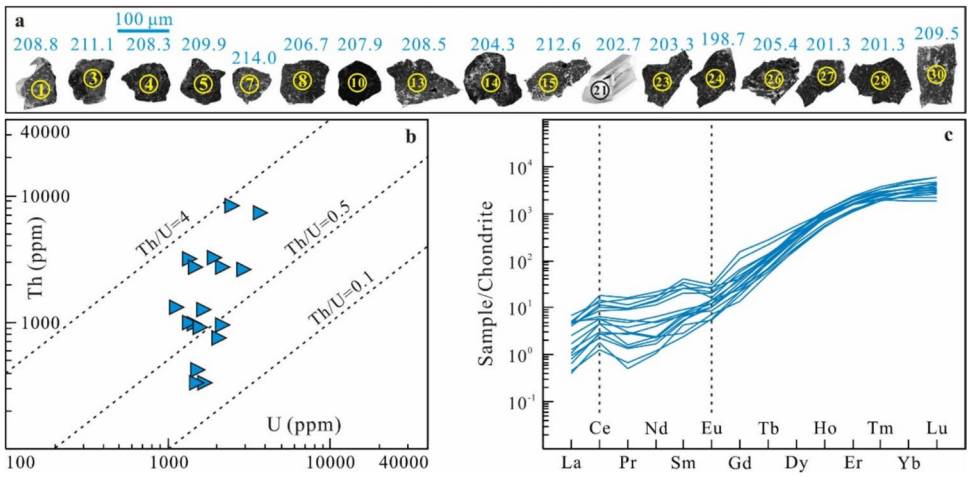

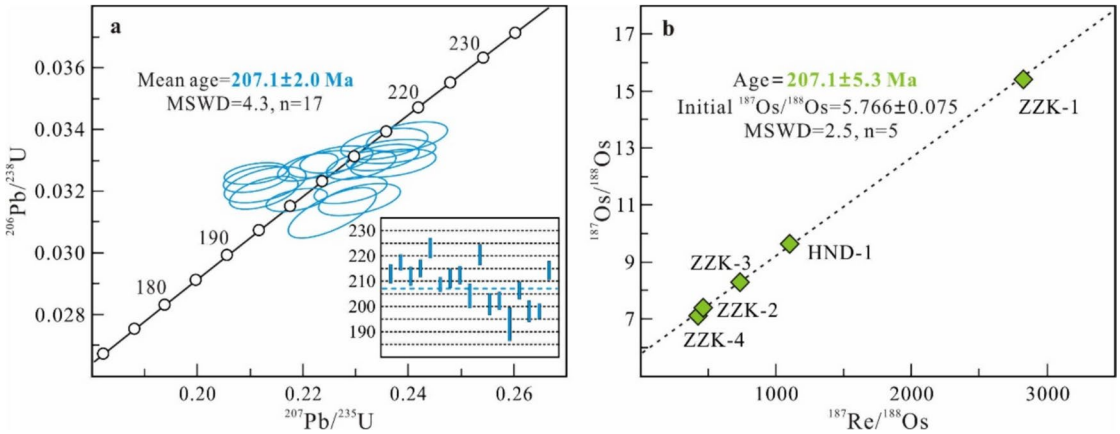

Fig. 5 **a** Cathodoluminescent images of the dating sample SYL-1; **b** Th vs. U diagram; **c** chondrite-normalized REE patterns of the dated zircons, chondrite values after Taylor and Mclennan (1985)

Fig. 6 **a** zircon U-Pb concordia diagram and weighted mean age of the dated zircons; **b** chalcopyrite Re-Os isochron age for the stratiform Cu deposits

intrusion are dominated by magmatic origin, with negligible hydrothermal fingerprints.

Furthermore, medium-pressure Barrovian-type metamorphism was initiated at ca. 210–205 Ma because of crustal thickening and shortening, and peak metamorphism (600–410 °C and 8–3 kbar) throughout the whole SGO was recorded at ca. 204–190 Ma according to monazite U-Pb and garnet Sm-Nd ages (Huang et al. 2003a, b). In this article, we proposed that ca. 204–190 Ma peak metamorphism probably fingerprinted the morphology of magmatic zircons within the syenite intrusion and was responsible for their atypical cathodoluminescent images (Fig. 5a). However, due to extremely high closure temperature of zircons (974 °C, Cherniak and Watson 2001), their U-Pb isotope systematics remained undisturbed and thus yielded robust dating results. This is exemplified by anatectic zircons, which were formed by anatexis during regional peak metamorphism and show relatively weak luminescence and indistinct oscillatory zoning (e.g., Grant et al. 2009; Lei et al. 2024). Furthermore, the short time interval between magmatism and peak metamorphism signifies that they were related to the same tectonothermal event (Grant et al. 2009).

The Songpan-Ganze Ocean, a branch of the Paleo-Tethys Ocean, was finally closed during the Late Triassic (Yan et al. 2018a, b). This induced the Triassic orogeny, which involved crustal shortening and thickening and widespread emplacement of syn- to late-orogenic/post-collisional granites with ages of 220–200 Ma (Roger et al. 2010). The Late Triassic igneous rocks marked the last episode of orogenic magmatism in the SGO, after which this region entered into a post-orogenic setting (ca. 200–150 Ma, Roger et al. 2010). In this contribution, zircon U-Pb dating results reveal that the newly discovered syenite intrusion was formed at ca. 207 Ma (Fig. 6a), indubitably associated with 220–200 Ma syn- to late-orogenic/post-collisional tectonic regime in the SGO (Roger et al. 2010). This is also confirmed by the Rb versus (Y + Nb) discriminant diagram, which shows that all the rock samples are seated in the field of post-collisional

Table 4 Chalcopyrite Re-Os isotope data for stratiform Cu deposits in the Jianglang Dome

Sample name	Ore deposit	Orebody	Mineralization style	Sample mass (g)	Re (ppb)	±2σ	Os (ppb)	±2σ	$^{187}Re/^{188}Os$	±2σ	$^{187}Os/^{188}Os$	±2σ
ZZK-1	Zhongzui	Z1-1	Massive	0.6503	2.553	0.019	0.0044	0.0000	2827.9	30.0	15.424	0.059
ZZK-2	Zhongzui	Z1-1	Massive	0.6502	2.897	0.034	0.0302	0.0003	462.7	6.6	7.386	0.021
ZZK-3	Zhongzui	Z1-1	Massive	0.6504	2.364	0.007	0.0155	0.0001	734.8	7.6	8.284	0.026
ZZK-4	Zhongzui	Z2-1	Massive	0.6504	2.595	0.019	0.0296	0.0004	423.8	5.8	7.123	0.054
HND-1	Heiniudong	I3	Massive	0.6504	6.684	0.049	0.0293	0.0002	1102.8	11.4	9.640	0.020

setting (Fig. 8a). Moreover, Patiño Douce (1999) carried out experimental studies and established pressure discrimination diagrams, which show low-pressure formation conditions for the studied syenite rocks (Fig. 8b). This is in accord with their late-orogenic/post-collisional extension regime.

The rock samples have significantly high (Zr + Nb + Ce + Y) concentrations of 619–436 ppm (Table 1), comparable to those of typical A-type granitoids (> 350 ppm, Whalen et al. 1987). This is also illuminated by 10000×Ga/Al versus Nb and Ce diagrams (Fig. 8c, d). According to zircon saturation thermometry proposed by Boehnke et al. (2013), our rock samples yield temperatures of 740–684 °C with an average of 707 °C (Table 1). Besides, estimated based on the calibration of Watson et al. (2006), the dated zircons show Ti-in-zircon temperatures of 1001–708 °C with an average of 827 °C (Table 3). These data are compatible with high-temperature formation conditions of A-type granitoids (King et al. 1997). Previous studies indicated that A-type granitoids can be formed by: (1) fractional crystallization of mantle-derived mafic magmas (Eby 1992), (2) partial melting of a crustal source (Patiño Douce 1997), or (3) mixing of the two end members (Yang et al. 2008). On chondrite-normalized diagram and primitive mantle-normalized trace element spidergram (Fig. 4f, g), the syenite samples resemble the patterns of continental crust and thus indicate a dominantly crustal origin. Besides, our dated zircons were all derived from a continental provenance (Fig. 7a, b). These geochemical signatures are compatible with their extremely low Mg# values of 2.30–1.22 (Table 1), which could be significantly elevated by mantle components (Rapp and Watson 1995). Although there is a lack of isotopic evidence, CaO/Na_2O versus Al_2O_3/TiO_2 and Rb/Ba versus Rb/Sr diagrams collectively indicate a mixing of basalt-derived (about 20% – 40%) and pelite-derived melts for their magma source (Fig. 8e, f).

As mentioned above, previous works uncovered that the Triassic SGO involves significant shortening and subsequent crustal thickening of the orogenic wedge, and such thickened crust induced the emplacement of ca. 220–200 Ma syn- to late-orogenic granitoids (Roger et al. 2010). Together, the studied syenite intrusion was emplaced at ca. 207 Ma and exhibits a crustal derivation in the Late Triassic SGO, with negligible mantle components. This is in favor of the viewpoint that A-type granitoids formed by partial melting of a crustal source (e.g., Patiño Douce 1997).

6.2 Multistage epigenetic Cu mineralization in the Jianglang Dome

In the core of the Jianglang Dome, a suite of high-grade stratiform Cu deposits is hosted by the Liwu Group, which was assigned a latest Neoproterozoic age of ca. 553 Ma according to zircon U-Pb dating (Li et al. 2016). In the past

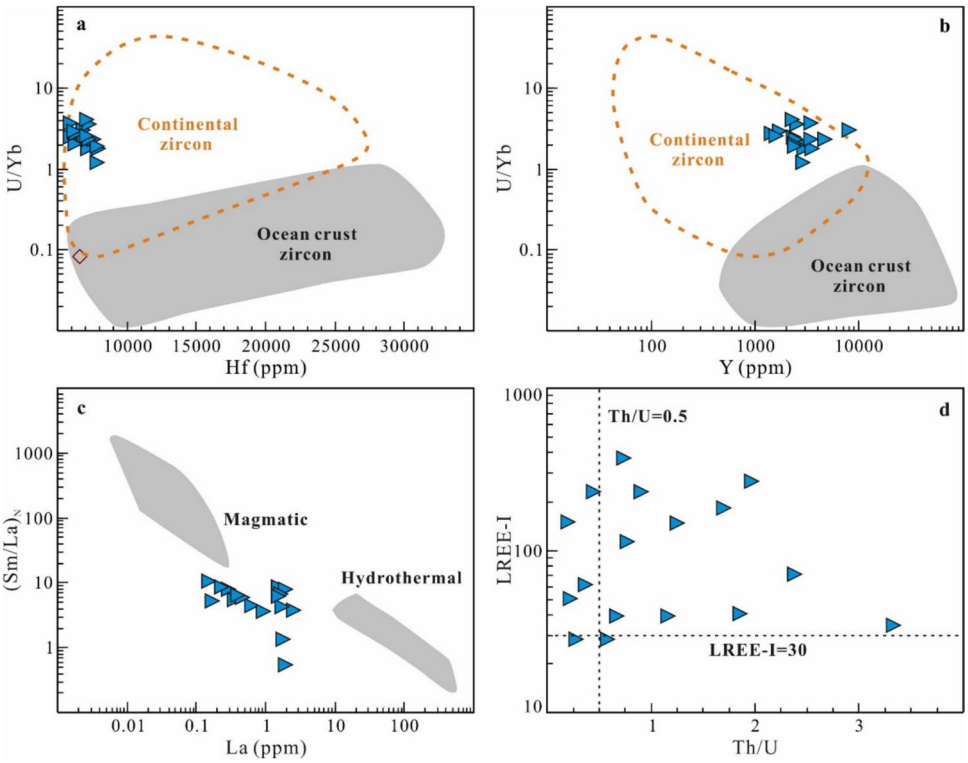

Fig. 7 Discriminant diagrams for the dated zircons. **a**, **b** U/Yb vs. Hf and Y diagrams (after Grimes et al. 2007); **c** $(Sm/La)_N$ vs. La diagram (after Hoskin 2005); **d** LREE-I vs. Th/U diagram

few decades, contrasting syngenetic (Yao 1990; Li et al. 2012) and epigenetic (Yan et al. 2003b; Ma et al. 2010; Chen et al. 2011; Zhou et al. 2017) models were proposed for stratiform Cu deposits in this area. Indeed, previous sulfur isotope data of metal sulfides ($\delta^{34}S_{V\text{-}CDT} = 8.7‰–5.6‰$, Yan et al. 1997) and boron isotope data of ore-associated tourmalines ($\delta^{11}B = -15.47‰ \pm 0.83‰$ to $-5.91‰ \pm 0.67‰$, Zhou et al. 2017) suggested a magmatic-hydrothermal affinity for regional stratiform Cu deposits. Furthermore, these deposits are closely associated with widespread hydrothermal alteration (Fig. 2e–g), probably indicating their epigenetic origin. However, robust age determinations are lacking because of the overall paucity of suitable minerals for isotopic dating.

Chalcopyrite Re-Os chronometers are widely used to date mineralization ages of sulfide deposits (e.g., Zhu and Sun et al. 2013). Zhou et al. (2017) first obtained a chalcopyrite Re-Os isochron age of 151.1 ± 4.8 Ma (2σ, $n = 5$, MSWD = 5.8) for the Liwu and Zhongzui deposits. This is likely suggestive of a post-magmatic hydrothermal origin (Zhou et al. 2017), associated with ca. 164 Ma Wenjiaping and Wulaxi granites (Dai et al. 2017). In this paper, five chalcopyrite separates yield an isochron age of 207.1 ± 5.3 Ma (MSWD = 2.5, Fig. 6b), which markedly postdates the formation age of their ore-hosting rocks (ca. 553 Ma, Li et al. 2016) and places a best estimate for another epigenetic mineralization age. The initial $^{187}Os/^{188}Os$ ratio of 5.766 ± 0.075 is higher than that of the upper continental crust (1.9–1.4, Peucker-Ehrenbrink and Jahn 2001) and indicates significant crustal contributions (e.g., Mathur et al. 2000; Chen et al. 2016; Soares et al. 2021). Our determinations thus suggest a crustal origin of metals, which is identical with the studied syenite intrusion. Noticeably, our dating result (ca. 207.1 Ma) contrasts the previously published Re-Os isochron age (ca. 151.1 Ma, Zhou et al. 2017). This is probably because of partial disturbance or resetting of Re-Os isotope systems (e.g., Nozaki et al. 2014; Muchez et al. 2015), induced by ca. 164 Ma granitic plutons in this region (Fig. 1b).

Perfectly, our new Re-Os age determination matches the emplacement age of the newly discovered syenite intrusion (207.1 ± 2.0 Ma, Fig. 6a) near the Zhongzui deposit (Fig. 1b), indicating ca. 207 Ma magmatic-hydrothermal mineralization. Considering chalcopyrite Re-Os age of ca. 151 Ma (Zhou et al. 2017), we propose multistage epigenetic mineralization for stratiform Cu deposits in the Jianglang Dome and advocate that ca. 207 Ma Cu mineralization event was overprinted by ca. 151 Ma category. Combined with age results as well as sulfide sulfur isotope ($\delta^{34}S_{V\text{-}CDT} = 8.7‰–5.6‰$, Yan et al. 1997) and tourmaline boron isotope ($\delta^{11}B = -15.47‰$ to $-5.91‰$, Zhou et al. 2017) data, these two mineralization events clearly show magmatic-hydrothermal affinities. According to the gravity data we have recently obtained in the core of the Jianglang

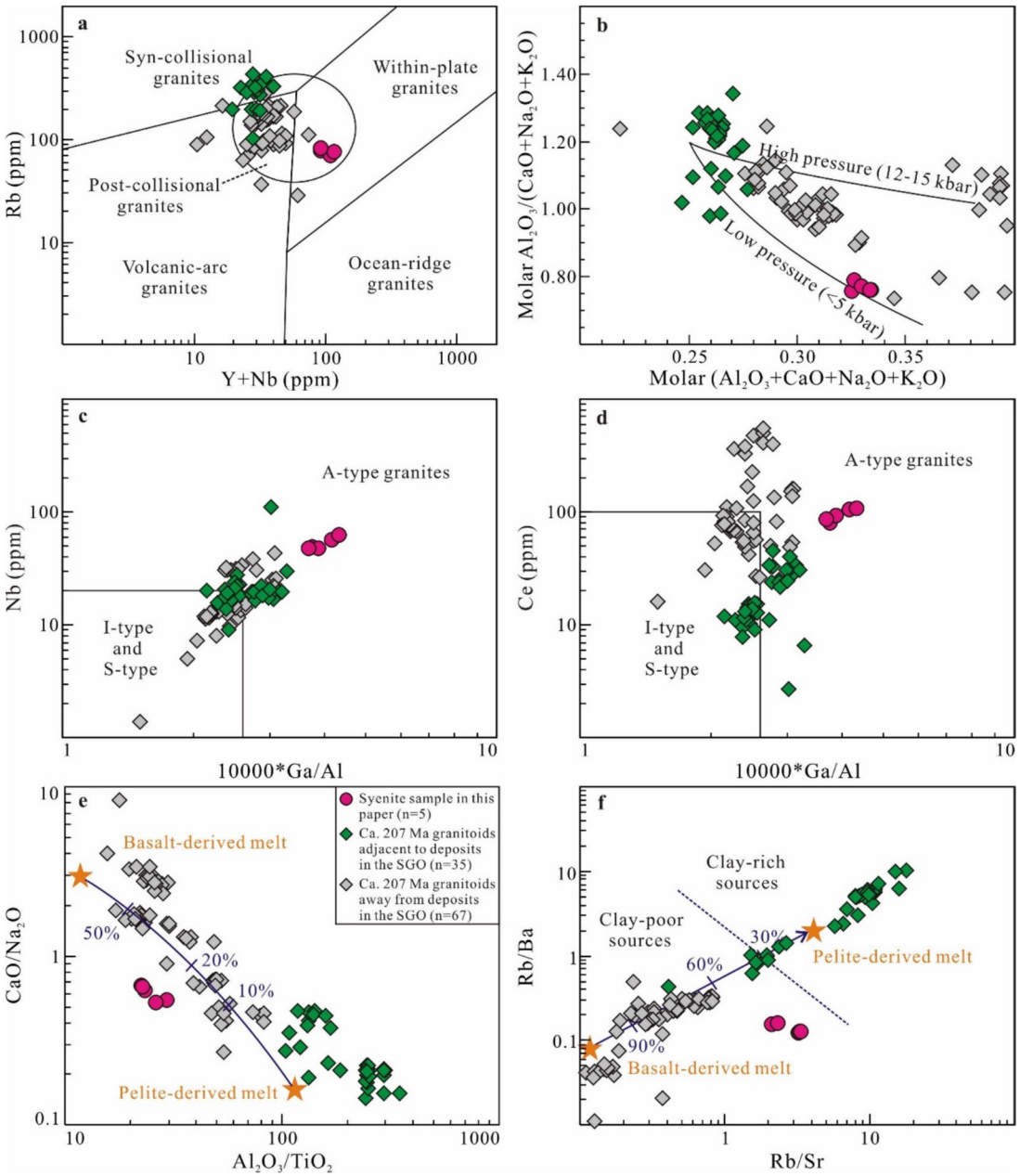

Fig. 8 **a** Rb vs. (Y + Nb) tectonic discrimination diagram (after Pearce et al. 1984); **b** Molar ($Al_2O_3 + CaO + Na_2O + K_2O$) vs. molar Al_2O_3/($CaO + Na_2O + K_2O$) pressure discrimination diagrams (after Patiño Douce 1999); **c**, **d** Nb and Ce vs. 10000×Ga/Al diagram (after Whalen et al. 1987); **e** Ca/Na_2O vs. Al_2O_3/TiO_2 diagram (after Patiño Douce and Harris 1998); **f** Rb/Ba vs. Rb/Sr diagram (after Patiño Douce 1999). Data sources as in Fig. 4

Dome, this region shows residual gravity low anomalies (Fig. 1c). This probably indicates a large deep-seated granitic batholith (e.g., Mangkhemthong et al. 2020) and further supports magmatic-hydrothermal mineralization in this area.

6.3 Regional comparison and rare metal mineralization potential

In recent decades, several giant rare metal deposits have been discovered in the SGO, e.g., Jiajika and Ke'eryin. These pegmatite-type deposits are probably associated with ca. 209–207 Ma granitoids in their vicinities (e.g., Li et al. 2022; Zhang et al. 2022). In this contribution, based

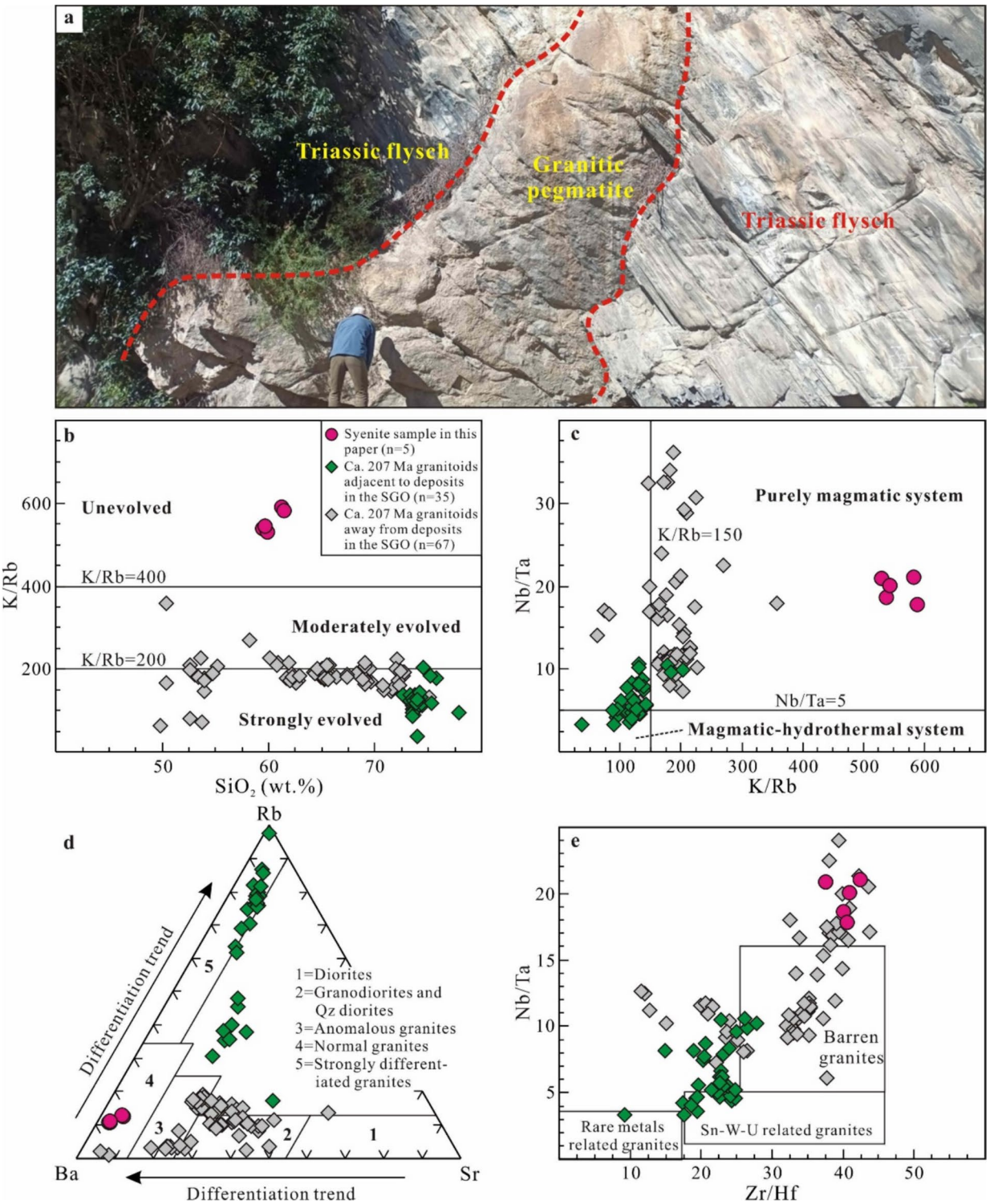

Fig. 9 **a** Granitic pegmatite veins intruding the Triassic strata in the Jianglang Dome; **b** K/Rb vs. SiO_2 diagram (after Blevin 2004); **c** Nb/Ta vs. K/Rb diagram (after Li et al. 2017); **d** Rb-Ba-Sr diagram (after Elbouseily and Elsokkary 1975); **e** Nb/Ta vs. Zr/Hf diagram (after Ballouard et al. 2016). Data sources as in Fig. 4

on zircon U-Pb dating, we assign a Late Triassic age (ca. 207 Ma, Fig. 6a) to the newly discovered syenite intrusion in the Jianglang Dome. This age is coeval with ca. 209–207 Ma granitoids related to rare metal mineralization in the SGO. Moreover, field investigation shows abundant granitic pegmatites intruded ancient strata in this region (Fig. 9a), likely indicating certain rare metal mineralization potential. For regional comparison, we select whole-rock geochemical data of (1) granitoids adjacent to rare metal deposits, including ca. 207 Ma Majingzi two-mica granite near Jiajika ($n = 21$, Zhang et al. 2022; Zhao et al. 2022) and ca. 209 Ma Ke'eryin aplite ($n = 14$, Li et al. 2022; Fei et al. 2023); (2) granitoids away from deposits, including ca. 205 Ma Taiyanghe monzonite ($n = 17$, Yuan et al. 2010; Deschamps et al. 2017), ca. 209 Ma Tagong monzogranite ($n = 15$, Chen et al. 2017), ca. 210–205 Ma Jinsha suture granodiorite ($n = 16$, Liu et al. 2019), and ca. 207 Ma Riluku monzogranite ($n = 19$, Zhan et al. 2020). These compiled granitoids (210–205 Ma, $n = 102$), together with our syenite samples ($n = 5$), show broadly consistent REE and trace element patterns (Fig. 4f–g) and a common post-collisional regime (Fig. 8a) as well as compositional heterogeneity (Fig. 4a–e and Fig. 8b–f).

Previous studies advocated that granitic pegmatites related to rare metal deposits were derived from evolved granitic systems via extreme differentiation (Roda-Robles et al. 2012; Hulsbosch et al. 2014). Blevin (2004) investigated metallogenic classification parameters for granitoid and related rocks of eastern Australia in detail and proposed that those granitoids with K/Rb ratios > 400 can be regarded as being compositionally unevolved. On K/Rb versus SiO_2 diagram, ca. 207 Ma granitoids adjacent to Jiajika and Ke'eryin rare metal deposits show strongly evolved signatures, while most granitoids away from deposits as well as our syenite samples are moderately evolved and unevolved (Fig. 9b). This is further illuminated by Nb/Ta versus K/Rb and Rb-Ba-Sr diagrams, which indicate strongly differentiated features for mineralization-related granitoids; however, a purely magmatic system without strong differentiation is suggested for another category (Fig. 9c, d). Using a compilation of published whole-rock geochemical data, Ballouard et al. (2016) uncovered that some immobile element ratios are good geochemical indicators of the fertility of granitic rocks. In this paper, the studied syenite samples show much higher Nb/Ta and Zr/Hf ratios, in contrast to fertile granitoids associated with Sn-W-U and rare metal mineralization (Fig. 9e). Taken together, the newly discovered syenite intrusion in the Jianglang Dome, with unevolved and barren affinities, exhibits negligible rare metal mineralization potential.

6.4 Implications for the nature of the Jianglang Dome

More than ten isolated domes were distributed in the eastern SGO, and they should be formed under a unified geodynamic background (Yan et al. 1997). To date, copper deposits with a certain scale have only been discovered in the core of the Jianglang Dome. Therefore, the genesis of this dome is critical to understanding the formation mechanism of stratiform Cu deposits in its core and even domal metamorphic bodies in the eastern SGO. However, the nature of the Jianglang Dome remains a matter of debate, including (1) a structural dome associated with overlapping of duplex compression and contraction (Hou 1996; Hou and Fu 2002) and (2) a metamorphic core complex related to magma-induced uplift caused by lithospheric thermal anomalies (Yan et al. 1997, 2003a).

Geophysical data indicate residual gravity low anomalies in the core of the Jianglang Dome (Fig. 1c), which is probably attributed to a large concealed granitic batholith in the deep (e.g., Mangkhemthong et al. 2020); however, direct evidence of igneous intrusions is lacking. Fortunately, the Late Triassic syenite intrusion was first discovered during our field geological mapping in this region (Fig. 2a–d). This probably suggests deep-seated granitoid batholith, which was responsible for thermal doming and multistage epigenetic Cu mineralization with magmatic-hydrothermal affinities in the Jianglang Dome (Yan et al. 1997; Zhou et al. 2017). Essentially, these geological events were all attributed to the Late Triassic post-collisional extension in the SGO (Roger et al. 2010; Huang et al. 2003a, b).

7 Conclusions

In this study, a syenite intrusion was first discovered in the core of the Jianglang Dome. It has an emplacement age of 207.1 ± 2.0 Ma, with A-type granite affinities and a crustal origin. This intrusion was attributed to the Late Triassic post-collisional extension in the SGO, and ca. 204–190 Ma peak metamorphism induced atypical morphological features of magmatic zircons. Selected from massive ores of regional stratiform Cu deposits, chalcopyrite Re–Os dating yields an isochron age of 207.1 ± 5.3 Ma and an elevated initial $^{187}Os/^{188}Os$ ratio of 5.766 ± 0.075, indicating epigenetic mineralization associated with the Late Triassic syenite intrusion.

Compared with ca. 209–207 Ma fertile granitoids in the SGO, the studied syenite intrusion shows unevolved and barren affinities and thus has insignificant rare metal mineralization potential. Synthesized with residual gravity low anomalies in the core of the Jianglang Dome, we prefer thermal doming as a result of magma-induced uplift for its formation mechanism.

Acknowledgements This research was financially supported by the National Natural Science Foundation of China (Nos. 41902068, 42272106), Young Scholars Development Fund of Southwest Petroleum University (No. 201499010083), and China Geological Survey Project (Nos. DD20230338, DD20242494). We are grateful to anonymous reviewers for their constructive comments and important corrections.

Author contributions YD and YZ conceived of the presented idea and contributed to the final manuscript; YD, YZ, and DX carried out the experiment; YD, HZ, SL, TL, and QZ carried out the field work.

Data availability The results from our study is our original unpublished work and it has not been submitted to any other journal for reviews. The data that support the findings of this study is available from the authors upon reasonable request.

Declarations

Conflict of interest The authors declare no conflict of interest.

Ethical approval This manuscript we wish to be considered for publication in ''Acta Geochimica''. No conflict of interest exits in the submission of this manuscript, and manuscript is approved by all authors for publication. I would like to declare on behalf of my co-authors that the work described was original research that has not been published previously, and not under consideration for publication elsewhere, in whole or in part. All the authors listed have approved the manuscript that is enclosed.

References

Ballouard C, Poujol M, Boulvais P, Branquet Y, Tartese R, Vigneresse JL (2016) Nb–Ta fractionation in peraluminous granites: a marker of the magmatic-hydrothermal transition. Geology 44(3):231–234. https://doi.org/10.1130/G37475.1

Bell EA, Boehnke P, Harrison TM (2016) Recovering the primary geochemistry of Jack Hills zircons through quantitative estimates of chemical alteration. Geochim Cosmochim Acta 191:187–202. https://doi.org/10.1016/j.gca.2016.07.016

Bell EA, Boehnke P, Barboni M, Harrison TM (2019) Tracking chemical alteration in magmatic zircon using rare earth element abundances. Chem Geol 510:56–71. https://doi.org/10.1016/j.chemgeo.2019.02.027

Blevin PL (2004) Redox and compositional parameters for interpreting the granitoid metallogeny of eastern Australia: Implications for gold-rich ore systems. Resour Geol 54:241–252. https://doi.org/10.1111/j.1751-3928.2004.tb00205.x

Boehnke P, Watson EB, Trail D, Harrison TM, Schmitt AK (2013) Zircon saturation re-revisited. Chem Geol 351:324–334. https://doi.org/10.1016/j.chemgeo.2013.05.028

Chen MH, Ding J, Chen DQ (2011) Origin of the ore-forming matter from the Liwu copper orefield in Jiulong. Sichuan Sediment Geol Tethyan Geol 31(1):89–93 (**in Chinese with English abstract**).

Chen K, Walker RJ, Rudnick RL, Gao S, Gaschnig RM, Puchtel IS, Tang M, Hu ZC (2016) Platinum-group element abundances and Re–Os isotopic systematics of the upper continental crust through time: evidence from glacial diamictites. Geochim Cosmochim Acta 191:1–16. https://doi.org/10.1016/j.gca.2016.07.004

Chen Q, Sun M, Zhao GC, Yang FL, Long XP, Li JH, Wang J, Yu Y (2017) Origin of the mafic microgranular enclaves (MMEs) and their host granitoids from the Tagong pluton in Songpan-Ganze terrane: an igneous response to the closure of the Paleo-Tethys ocean. Lithos 290–291:1–17. https://doi.org/10.1016/j.lithos.2017.07.019

Cherniak DJ, Watson EB (2001) Pb diffusion in zircon. Chem Geol 172:1999–2017. https://doi.org/10.1016/S0009-2541(00)00233-3

Dai YP, Zhang HH, Zhu YD, Shen ZW, Li TZ, Ma D (2016) Review on Jianglang dome and Liwu-type copper deposit in the western margin of Yangtze block. J Earth Sci Environ 38(1):66–78 (**in Chinese with English abstract**).

Dai YP, Zhu YD, Li TZ, Zhang HH, Tang GL, Shen ZW (2017) A crustal source for ca. 165 Ma post-collisional granites related to mineralization in the Jianglang dome of the Songpan-Ganzi Orogen, eastern Tibetan Plateau. Chem Erde-Geochem 77:573–586. https://doi.org/10.1016/j.chemer.2017.10.004

Deschamps F, Duchene S, Sigoyer J, Bosse V, Benoit M, Vanderhaeghe O (2017) Coeval mantle-derived and crust-derived magmas forming two neighbouring plutons in the Songpan-Ganze accretionary orogenic wedge (SW China). J Petrol 58(11):2221–2256. https://doi.org/10.1093/petrology/egy007

Du AD, Wu SQ, Sun DZ, Wang SX, Qu WJ, Markey R, Stein H, Morgan J, Malinovskiy D (2004) Preparation and certification of Re–Os dating reference materials: Molybdenites HLP and JDC. Geostand Geoanal Res 28:41–52. https://doi.org/10.1111/j.1751-908X.2004.tb01042.x

Du AD, Qu WJ, Wang DH, Li C (2012) Application of the Re–Os dating in economic geology. Beijing: Geological Publishing House, 1–182 (in Chinese).

Eby GN (1992) Chemical subdivision of the A-type granitoids: Petrogenetic and tectonic implications. Geology 20:641–644. https://doi.org/10.1130/0091-7613(1992)020%3c0641:CSOTAT%3e2.3.CO;2

Elbouseily AM, Elsokkary AA (1975) Relation between Rb, Ba and Sr in granitic rocks. Chem Geol 16:207–219. https://doi.org/10.1016/0009-2541(75)90029-7

Fei GC, Li TR, Menuge JF, Hui ZQ, Yuan YW, Zhu HP, Tan H, Cai YH, Tang WC, Yang GB, Luo XL, Chen ZP, Chen X, Yun H (2023) Petrogenesis of aplites in the Ke'eryin rare metal orefield in the Songpan-Garze Fold Belt, Eastern Tibet: evidence from mineralogy, geochemistry, geochronology and Hf-Nd isotopes. Lithos 438–439:107017. https://doi.org/10.1016/j.lithos.2023.107017

Grant ML, Wilde SA, Wu FY, Yang JH (2009) The application of zircon cathodoluminescence imaging, Th–U–Pb chemistry and U–Pb ages in interpreting discrete magmatic and high-grade metamorphic events in the North China Craton at the Archean/Proterozoic boundary. Chem Geol 261(1–2):155–171. https://doi.org/10.1016/j.chemgeo.2008.11.002

Grimes CB, John BE, Kelemen PB, Mazdab FK, Wooden JL, Cheadle MJ, Hanghøj K, Schwartz JJ (2007) Trace element chemistry of zircons from oceanic crust: a method for distinguishing detrital zircon provenance. Geology 35(7):643–646. https://doi.org/10.1130/G23603A.1

Horstwood MSA, Košler J, Gehrels G, Jackson SE, McLean NM, Paton C, Pearson NJ, Sircombe K, Sylvester P, Vermeesch P, Bowring JF, Condon DJ, Schoene B (2016) Community-derived standards for LA-ICP-MS U-(Th-)Pb geochronology-uncertainty propagation, age interpretation and data reporting. Geostand Geoanal Res 40:311–332. https://doi.org/10.1111/j.1751-908X.2016.00379.x

Hoskin PWO (2005) Trace-element composition of hydrothermal zircon and the alteration of Hadean zircon from the Jack Hills, Australia. Geochim Cosmochim Acta 69:637–648. https://doi.org/10.1016/j.gca.2004.07.006

Hoskin PWO, Schaltegger U (2003) The composition of zircon and igneous and metamorphic petrogenesis. Rev Mineral Geochem 53:27–62. https://doi.org/10.2113/0530027

Hou LW (1996) Type and origin of the core complexes and the domal deformational-metamorphic bodies in the western margin of Yangtze craton. Acta Geologica Sichuan 16(1):6–11 (**in Chinese with English abstract**).

Hou LW, Fu XF (2002) Domal metamorphic bodies in the eastern margin of the Songpan-Ganze orogenic belt. Chengdu: Sichuan University Press, 1–163 (in Chinese).

Huang MH, Buick IS, Hou LW (2003a) Tectonometamorphic evolution of the eastern Tibet Plateau: Evidence from the central east Songpan-Garze orogenic belt, western China. J Petrol 44:225–278. https://doi.org/10.1093/petrology/44.2.255

Huang MH, Maas R, Buick IS, Williams IS (2003b) Crustal response to continental collisions between the Tibet, Indian, South China and North China blocks: Geochronological constraints from the Songpan-Garze orogenic belt, western China. J Metamorph Geol 21:223–240. https://doi.org/10.1046/j.1525-1314.2003.00438.x

Hulsbosch N, Hertogen J, Dewaele S, AndréL MP (2014) Alkali metal and rare earth element evolution of rockforming minerals from the Gatumba area pegmatites (Rwanda): quantitative assessment of crystal-melt fractionation in the regional zonation of pegmatite groups. Geochim Cosmochim Acta 132:349–374. https://doi.org/10.1016/j.gca.2014.02.006

Irvine T, Baragar W (1971) A guide to the chemical classification of the common volcanic rocks. Can J Earth Sci 8:523–548. https://doi.org/10.1139/e71-055

King PL, White AJR, Chappell BW, Allen CM (1997) Characterization and origin of aluminous A-type granites from the Lachlan Fold Belt, Southeastern Australia. J Petrol 38:371–391. https://doi.org/10.1093/petroj/38.3.371

Le Maitre RW (2002) Igneous rocks, a classification and glossary of terms. Cambridge University Press, Cambridge, pp 1–236.

Lei HC, Xu HJ, Zhang H, Deng LP, Hu DS, Ye YK (2024) From Triassic metamorphism to Early Cretaceous anatexis in the Dabie orogen, central China: constraints from in-situ U–Pb age and Hf and O isotopes of zircon from migmatites. J Asian Earth Sci 265:106107. https://doi.org/10.1016/j.jseaes.2024.106107

Li JZ, Liu YP, Shen ZW, Ma GT, Zhu XP, Tang GL (2012) Geological characteristics, genesis and metallogenic time of the Heiniudong copper-zinc deposit in Jiulong county Sichuan Province. Acta Geologica Sinica 86(12):1972–1993 (**in Chinese with English abstract**).

Li TZ, Dai YP, Zhou Q, Zhang HH, Feng XL, Ma D, Shen ZW (2016) Formation age and tectonic setting of the Liwu Group at the core of Jianglang Dome in the western margin of Yangtze Block. Acta Geol Sin 90(10):2551–2566 (**in Chinese with English abstract**).

Li YHM, Zhao WW, Zhou MF (2017) Nature of parent rocks, mineralization styles and ore genesis of regolith-hosted REE deposits in South China: an integrated genetic model. J Asian Earth Sci 148:65–95. https://doi.org/10.1016/j.jseaes.2017.08.004

Li X, Dai HZ, Wang DH, Liu SB, Wang GH, Wang CH, Huang F, Zhu HY (2022) Geochronological and geochemical constraints on magmatic evolution and mineralization of the northeast Ke'eryin pluton and the newly discovered Jiada pegmatite-type lithium deposit. West China Ore Geol Rev 150:105164. https://doi.org/10.1016/j.oregeorev.2022.105164

Liu YS, Hu ZC, Gao S, Günther D, Xu J, Gao CG, Chen HH (2008) In situ analysis of major and trace elements of anhydrous minerals by LA-ICP-MS without applying an internal standard. Chem Geol 257:34–43. https://doi.org/10.1016/j.chemgeo.2008.08.004

Liu Y, Xiao WJ, Windley BF, Li RS, Ji WH, Zhou KF, Sang M, Chen YC, Jia XL, Li L, Zhang HD (2019) Late Triassic ridge subduction of Paleotethys: insights from high-Mg granitoids in the Songpan-Ganzi area of northern Tibet. Lithos 334–335:254–272. https://doi.org/10.1016/j.lithos.2019.03.012

Ma GT, Ma DF, Gao DF, Wang MJ, Li JZ, Yao P, Zhu XP, Chen MH, Liang J (2010) Geology and genesis of the Heiniudong copper-zinc deposit in Jiulong. Sichuan Sediment Geol Tethyan Geol 30(2):84–90 (**in Chinese with English abstract**).

Mangkhemthong N, Morley CK, Kanthiya S, Chaisri S (2020) Geological model and development of the Cenozoic Wiang Pa Pao Basin, Chiang Rai Province, Northern Thailand, based on gravity data modelling and surface structural interpretation. Tectonophysics. https://doi.org/10.1016/j.tecto.2020.228454

Mathur R, Ruiz J, Munizaga F (2000) Relationship between copper tonnage of Chilean base-metal porphyry deposits and Os isotope ratios. Geology 28(6):555–558. https://doi.org/10.1130/0091-7613(2000)28%3c555:RBCTOC%3e2.0.CO;2

Middlemost EAK (1994) Naming materials in the magma/igneous rock system. Earth Sci Rev 37:215–224. https://doi.org/10.1016/0012-8252(94)90029-9

Muchez P, André-Mayer AS, El Desouky HA, Reisberg L (2015) Diagenetic origin of the stratiform Cu–Co deposit at Kamoto in the central African copperbelt. Miner Depos 50:437–447. https://doi.org/10.1007/s00126-015-0582-3

Nozaki T, Kato Y, Suzuki K (2014) Re–Os Geochronology of the Hitachi volcanogenic massive sulfide deposit: the oldest ore deposit in Japan. Econ Geol 109:2023–2034. https://doi.org/10.2113/econgeo.109.7.2023

Patiňo Douce AE (1997) Generation of metaluminous A-type granites by low-pressure melting of calc-alkaline granitoids. Geology 25:743–746. https://doi.org/10.1130/0091-7613(1997)025%3c0743:GOMATG%3e2.3.CO;2

Patiňo Douce AE (1999) What do experiments tell us about the relative contributions of crust and mantle to the origin of granitic magmas? Geol Soc Lond Spec Publ 168:55–75. https://doi.org/10.1144/GSL.SP.1999.168.01.05

Patiňo Douce AE, Harris N (1998) Experimental constraints on Himalayan anatexis. J Petrol 39:689–710. https://doi.org/10.1093/petroj/39.4.689

Pearce JA, Harris NBW, Tindle AG (1984) Trace element discrimination diagrams for the tectonic interpretation of granitic rocks. J Geol 25:956–983. https://doi.org/10.1093/petrology/25.4.956

Peccerillo A, Taylor SR (1976) Geochemistry of Eocene calc-alkaline volcanic rocks from the Kastamonu area, Northern Turkey. Contrib Tomineral Petrol 58:63–81. https://doi.org/10.1007/BF00384745

Peucker-Ehrenbrink B, Jahn B (2001) Rhenium-osmium isotope systematics and platinum group element concentrations: loess and the upper continental crust. Geochem Geophys Geosyst. https://doi.org/10.1029/2001GC000172

Rapp RP, Watson EB (1995) Dehydration melting of metabasalt at 8–32 kbar: implications for continental growth and crust-mantle recycling. J Petrol 36:891–931. https://doi.org/10.1093/petrology/36.4.891

Roda-Robles E, Pesquera A, Gil-Crespo PP, Torres-Ruiz J (2012) From granite to highly evolved pegmatite: a case study of the Pinilla de Fermoselle granite–pegmatite system (Zamora, Spain). Lithos 153:192–207. https://doi.org/10.1016/j.lithos.2012.04.027

Roger F, Jolivet M, Malavieille J (2010) The tectonic evolution of the Songpan-Garzê (North Tibet) and adjacent areas from Proterozoic to Present: a synthesis. J Asian Earth Sci 39:254–269. https://doi.org/10.1016/j.jseaes.2010.03.008

Sláma J, Košler J, Condon DJ, Crowley JL, Gerdes A, Hanchar JM, Horstwood MSA, Morris GA, Nasdala L, Norberg N, Schaltegger U, Xchoene B, Tubrett MN, Whitehouse MJ (2008) Plešovice zircon: a new natural reference material for U–Pb and Hf isotopic

microanalysis. Chem Geol 249:1–35. https://doi.org/10.1016/j.chemgeo.2007.11.005
Soares MB, Selby D, Robb L, Neto AVC (2021) Sulfide recrystallization and gold remobilization during the 2.0 ga stage of the Minas orogeny: implications for gold mineralization in the Quadrilátero Ferrífero area, Brazil. Econ Geol 116(6):1455–1466. https://doi.org/10.5382/econgeo.4830
Streckeisen A, Le Maitre RW (1979) A chemical approximation to the modal QAPF classification of the igneous rocks. Neues Jb Mineral Abh 136:169–206.
Sun SS, McDonough WF (1989) Chemical and isotopic systematics of oceanic basalts: implications for mantle composition and processes. Geol Soc Lond Spec Publ 42:313–345. https://doi.org/10.1144/GSL.SP.1989.042.01.19
Taylor SR, Mclennan SM (1985) The continental crust: Its composition and evolution. Blackwell Scientific Publications, Oxford, pp 1–312.
Vermeesch P (2018) IsoplotR: a free and open toolbox for geochronology. Geosci Front 9:1479–1493. https://doi.org/10.1016/j.gsf.2018.04.001
Watson EB, Wark DA, Thomas JB (2006) Crystallization thermometers for zircon and rutile. Contrib Miner Petrol 151:413–433. https://doi.org/10.1007/s00410-006-0068-5
Weislogel AL, Graham SA, Chang EZ, Wooden JL, Gehrels GE (2010) Detrital zircon provenance from three turbidite depocenters of the Middle-Upper Triassic Songpan-Ganzi complex, central China: record of collisional tectonics, erosional exhumation, and sediment production. Geol Soc Am Bull 122:2041–2062. https://doi.org/10.1130/B26606.1
Whalen JB, Currie KL, Chappel BW (1987) A-type granites: geochemical characteristics, discrimination and petrogenesis. Contrib Miner Petrol 95:407–419. https://doi.org/10.1007/BF00402202
Yan DP, Zhou MF, Song HL, Fu ZR (2003a) Structural style and tectonic significance of the Jianglang dome in the eastern margin of the Tibetan Plateau, China. J Struct Geol 25:765–779. https://doi.org/10.1016/S0191-8141(02)00059-7
Yan DP, Zhou MF, Song HL, Fu ZR, Sun M (2003b) Tectonic controls on the formation of the Liwu Cu-rich sulfide deposit in the Jianglang Dome, SW China. Resour Geol 53:89–100. https://doi.org/10.1111/j.1751-3928.2003.tb00161.x
Yan DP, Qiu L, Wells ML, Zhou MF, Meng X, Lu S, Zhang S, Wang Y, Li SB (2018a) Structural and geochronological constraints on the early Mesozoic north Longmen Shan Thrust Belt: Foreland fold-thrust propagation of the SW Qinling orogenic belt, northeastern Tibetan plateau. Tectonics 37:4595–4624. https://doi.org/10.1029/2018TC004986
Yan DP, Zhou Y, Qiu L, Wells ML, Mu HX, Xu CG (2018b) The Longmenshan Tectonic Complex and adjacent tectonic units in the eastern margin of the Tibetan Plateau: A review. J Asian Earth Sci 164:33–57. https://doi.org/10.1016/j.jseaes.2018.06.017
Yan DP, Song HL, Fu ZR, Tian JY (1997) Metamorphic core complexes in the western margin of the Yangtze platform. Beijing: Geological Publisher House, 1–94 (in Chinese with English abstract).
Yang JH, Wu FY, Wilde SA, Zhao GC (2008) Petrogenesis and geodynamics of Late Archean magmatism in eastern Hebei, eastern North China Craton: geochronological, geochemical and Nd–Hf isotopic evidence. Precambr Res 167:125–149. https://doi.org/10.1016/j.precamres.2008.07.004
Yao JD (1990) Genesis of the Liwu copper deposit. Acta Geologica Sichuan 10(4):251–258 (**in Chinese**).
Yuan C, Zhou MF, Sun M, Zhao YJ, Wilde S, Long XP, Yan DP (2010) Triassic granitoids in the eastern Songpan Ganzi Fold Belt, SW China: magmatic response to geodynamics of the deep lithosphere. Earth Planet Sci Lett 290:481–492. https://doi.org/10.1016/j.epsl.2010.01.005
Zhan QY, Zhu DC, Wang Q, Weinberg RF, Xie JC, Li SM, Zhang LL, Zhao ZD (2020) Source and pressure effects in the genesis of the Late Triassic high Sr/Y granites from the Songpan-Ganzi Fold Belt, eastern Tibetan Plateau. Lithos 368–369:105584. https://doi.org/10.1016/j.lithos.2020.105584
Zhang HF, Parrish P, Zhang L, Xu WC, Yuan HL, Gao S, Crowley QG (2007) A-type granite and adakitic magmatism association in Songpan-Garze fold belt, eastern Tibetan Plateau: Implication for lithospheric delamination. Lithos 97:323–335. https://doi.org/10.1016/j.lithos.2007.01.002
Zhang HJ, Tian SH, Wang DH, Liu T, Li XF, Zhang YJ, Fu XF, Hao XF, Hou KJ, Zhao Y, Qin Y (2022) Lithium isotopic constraints on the petrogenesis of the Jiajika two-mica granites and associated Li mineralization. Ore Geol Rev 150:105174. https://doi.org/10.1016/j.oregeorev.2022.105174
Zhao H, Chen B, Huang C, Bao C, Yang Q, Cao R (2022) Geochemical and Sr–Nd–Li isotopic constraints on the genesis of the Jiajika Li-rich pegmatites, eastern Tibetan Plateau: Implications for Li mineralization. Contrib Miner Petrol 177:4. https://doi.org/10.1007/s00410-021-01869-3
Zhou Q, Li WC, Zhang HH, Li TZ, Yuan HY, Feng XL, Li C, Liao ZW, Wang SW (2017) Post-magmatic hydrothermal origin of late Jurassic Liwu copper polymetallic deposits, western China: direct chalcopyrite Re–Os dating and Pb–B isotopic constraints. Ore Geol Rev 89:526–543. https://doi.org/10.1016/j.oregeorev.2017.07.008
Zhu ZM, Sun YL (2013) Direct Re–Os dating of chalcopyrite from the Lala IOCG deposit in the Kangdian copper belt, China. Econ Geol 108:871–882. https://doi.org/10.2113/econgeo.108.4.871
Zhu YD, Dai YP, Wang LL, Xiu D, Chen C (2020) Geochemical and isotopic compositions of Late Permian metavolcano-sedimentary sequence in the southern Songpan-Ganzi Orogen, eastern Tibetan Plateau. Geol Mag 157:2004–2020. https://doi.org/10.1017/S0016756820000230